Nanocrystalline graphene for ultrasensitive surface-enhanced Raman spectroscopy

Applied Surface Science xxx (xxxx) 154035

Contents lists available at ScienceDirect

Applied Surface Science

journal homepage: www.elsevier.com/locate/apsusc

Full Length Article

Nanocrystalline graphene for ultrasensitive surface-enhanced Raman spectroscopy

Giuliana Faggio [a,*], Rossella Grillo [a,*], Nicola Lisi [b], Francesco Buonocore [b], Rosa Chierchia [b], Min Jung Kim [d], Gwan-Hyoung Lee [e,f,g,h], Andrea Capasso [c,*], Giacomo Messina [a]

[a] Department of Information Engineering, Infrastructures and Sustainable Energy (DIIES), University "Mediterranea" of Reggio Calabria, Loc. Feo di Vito, 89122 Reggio Calabria, Italy
[b] Agenzia nazionale per le nuove tecnologie, l'energia e lo sviluppo economico sostenibile (ENEA), Casaccia Research Centre, Roma 00123, Italy
[c] International Iberian Nanotechnology Laboratory (INL), Braga 4715-330, Portugal
[d] Department of Material Science and Engineering, Yonsei University, Seoul, 03722, Republic of Korea
[e] Department of Materials Science and Engineering, Seoul National University, Seoul 08826, Republic of Korea
[f] Research Institute of Advanced Materials (RIAM), Seoul National University, Seoul 08F826, Republic of Korea
[g] Institute of Engineering Research, Seoul National University, Seoul 08826, Republic of Korea
[h] Institute of Applied Physics, Seoul National University, Seoul 08826, Republic of Korea

ARTICLE INFO

Keywords:
2D materials
Surface-enhanced Raman spectroscopy
SERS
Nanocrystalline graphene
Graphene enhanced Raman spectroscopy
GERS
Charge transfer

ABSTRACT

The development of ultrasensitive and biocompatible Surface-Enhanced Raman Spectroscopy (SERS) substrates, able to provide uniform and reproducible signals, has become a focus of study in the last decade. Graphene, with his advantageous properties, such as photoluminescence quenching of fluorescent dyes, chemical inertness and biocompatibility, allows to overcome many important limitations of conventional metal SERS substrates. In this work, we develop ultrasensitive graphene substrates by ethanol Chemical Vapor Deposition (CVD). Large-area thin films composed of nanosized sp^2 grains surrounded by disordered regions are obtained by lowering the growth temperature from the standard 1070 °C to 700 °C. Our substrates are able to detect trace amounts of molecules, down to $6{\cdot}10^{-11}$ M, which is the lowest concentration that has been achieved in Graphene-Enhanced Raman Spectroscopy (GERS) with rhodamine 6G (R6G) as probe molecule. This outstanding result is attributable to two main features: i) more efficient charge transfer due to the energy level matching between R6G and the nanocrystalline graphene film; ii) large number of grain boundaries acting as "trapping sites" for the molecules.

1. Introduction

Surface-Enhanced Raman Spectroscopy (SERS) has attracted increasing attention as one of the most efficient analytical techniques for single-molecule detection [1–3]. SERS is a surface-sensitive technique that allows a significant amplification of weak Raman scattering signals originating from molecules adsorbed on a substrate, typically rough or nanostructured metal surfaces [2]. A signal amplification of several orders of magnitudes (8–14) has been achieved by exploiting the electromagnetic field enhancement properties of the substrates [4–7]. The signal enhancement in SERS originates from two main contributions: the electromagnetic and the chemical mechanisms [1,8–10]. The electromagnetic mechanism (EM) that has dominant contribution to signal enhancement is due to a strong amplification of the local electromagnetic fields near the metal nanostructures [8,10]. The chemical mechanism (CM) is ascribed to the electron transfer between the substrate and the adsorbed molecules [11]. The charge transfer occurs only when the molecule is in contact or very close to the substrate with a distance smaller than 0.2 nm [12], which is the reason why the CM is termed as a "first layer effect" [13]. However, the signal enhancement by the CM is typically $10–10^2$, several orders of magnitude lower than that by the EM [11]. Because the total SERS enhancement is the product of EM and CM [14], coexistence of these two enhancement mechanisms makes the SERS extremely sensitive for a single-molecule detection [14]. Nevertheless, the SERS has limits in practical application. For example, the sensitivity of the SERS is considerably small for fluorescent molecules because the Raman signals are hidden under broad fluorescence spectrum, being the cross section of fluorescence much larger than that of the Raman scattering [15,16]. In addition, an important weakness of

* Corresponding authors.
E-mail addresses: gfaggio@unirc.it (G. Faggio), rossella.grillo@unirc.it (R. Grillo), andrea.capasso@inl.int (A. Capasso).

https://doi.org/10.1016/j.apsusc.2022.154035
Received 5 April 2022; Received in revised form 9 June 2022; Accepted 20 June 2022
0169-4332/

conventional metal SERS substrates is the difficulty in providing uniform and reproducible signals [12].

Graphene, a monolayer carbon sheet with honeycomb crystal structure, could serve as ideal SERS substrate for three main reasons [11]. i) Fluorescent molecules adsorbed on graphene usually undergo a significant photoluminescence (PL) quenching with a factor up to ~10^3 [17], which enables to obtain clearly discernable Raman signals [17]. ii) graphene is chemically inert so that there is no significant alteration of the electronic structure in the adsorbed molecules [18], but only an increase of the molecular polarizability, which is in contrast to chemically active metal substrates that form chemical bonds with the adsorbed molecules [11]. Thus, the molecules on the graphene preserves their Raman fingerprints with enhanced Raman intensities. iii) Biological compatibility of graphene extends the application fields of SERS to biosensing and drug delivery [11,19–21]. The Raman signal enhancement by using a graphene substrate, termed Graphene-Enhanced Raman Spectroscopy (GERS), has been widely investigated in the last years and ascribed to the CM [11,18,22–24]. Since the EM generally requires noble metal substrates (such as silver, gold and copper) with rough or nanostructured surfaces that can effectively absorb the incident laser light (usually in the visible range) and generate surface plasmons, atomically flat graphene surface with low optical absorption of 2.3% and a surface plasmon in the THz region is not appropriate for the EM [12,11].

Recently, considerable efforts have been devoted to clarify the fundamental mechanisms of two-dimensional (2D) CM-based SERS effect and to further increase its sensitivity [25]. Femtomolar and sub-femtomolar (~10^{-16} M) detection for R6G molecules has been reported in 2D transition-metal dichalcogenides (monolayer to few-layer $NbSe_2$) and 2D van der Waals heterostructures (graphene/ReO_xS_y) [26–28]. Such ultrasensitive SERS effect has been attributed to the strong adsorption energy and efficient charge transfer between the R6G molecules and the substrate together with large DOS at the Fermi level, which increases the charge transfer probability inducing outstanding Raman enhancement [26–28]. In the framework of graphene-based materials, mechanically exfoliated graphene [11,29], graphene oxide [30–32], CVD doped graphene [25,31] have been largely used as GERS substrates. It has been reported that the edges of quantum dots, nanomesh, and graphene nanoribbons are the main sites that greatly improve GERS sensitivity [33–36]. Among the different graphene types, CVD graphene films offer the advantage of continuous GERS substrates over large areas. Moreover, CVD graphene is typically polycrystalline and thus particularly suited for GERS, due to the high density of grain boundaries [33–36]. Previously, we studied the CVD growth of polycrystalline graphene by using ethanol as precursor and showed the effect of the CVD temperature on the grain size control (from hundreds to a few nm) [37]. In this work, we produced ultrasensitive SERS substrates based on graphene films grown by ethanol CVD. At present, the lowest detection limit obtained in graphene-based materials for rhodamine 6G (R6G) molecules is 10^{-8} M and 10^{-10} M, achieved by using CVD N-doped graphene [25] and exfoliated graphene [11] as substrates, respectively. To further increase the sensitivity, we fabricated nanocrystalline films composed of nanocrystalline sp^2 grains of 5–20 nm surrounded by disordered regions (CVD temperature ranging from 700 to 860 °C) [38]. The Raman signal intensity originating from the R6G molecules was found to increase at smaller graphene grain sizes. We were able to detect extremely low level of R6G molecules, down to $6{\cdot}10^{-11}$ M, which is the lowest concentration that has been achieved in GERS for R6G molecules. The high GERS sensitivity of nanocrystalline graphene films is attributed to two main features: i) increased work function that allows for an effective charge transfer by energy level matching between the probing molecule and graphene; ii) increase of grain boundaries, which act as "trapping sites" for the molecules. Our work shows great potential of the nanocrystalline graphene films grown by ethanol CVD at low temperature for GERS in detection of Raman signals at single-molecule level. We demonstrate that nanostructured SERS platforms based on chemical mechanism can be engineered by simply tuning the CVD growth temperature.

2. Experimental and theoretical results

2.1. Structural and morphological investigation of the GERS substrates

The morphology of the CVD graphene films was investigated by HR-TEM and Raman spectroscopy. The Gr1070, Gr860 and Gr700 indicate the graphene films grown at different temperatures of 1070, 860, and 700 °C, respectively. As we previously reported, the samples maintain the 2D geometry but have a different microstructure, which are composed of crystalline grains and disordered regions [37]. Raman analysis showed that only Gr1070 is highly crystalline with very low defect density, while Gr860 and Gr700 exhibited large amount of defects (**Figure S1**). HR-TEM image of Fig. 1**a and b** show that Gr860 is a continuous film composed of nanocrystalline grains with an average size of ~20 nm surrounded by disordered regions. The Gr700 showed drastically reduced average grain size of ~5 nm and predominant disordered regions, as shown in Fig. 1**c and d**. The Gr860 sample contains crystalline grains with an average size of ~20 nm, as confirmed by the bright spots with six-fold symmetry in the fast Fourier transform (FFT) in Fig. 1**b** (inset). Meanwhile, the Gr700 sample shows smaller crystalline grains with an average size of ~5 nm, resulting in a FFT with ring-like patterns made of multiple spots (Fig. 1**d**, inset). As expected, a higher growth temperature leads to samples with larger crystalline grains. As previously reported, the Gr1070 [39,40] exhibited well-stitched crystalline graphene film without any disordered regions. Absence of D peak in the Raman spectra of Gr1070 also supports that the higher crystallinity is achieved for the graphene grown at higher temperature (**Figure S1**).

Surface morphology of Gr860 and Gr700 samples were investigated using atomic force microscopy (AFM) as shown in **Figure S2**. The Gr860 and Gr700 showed thicknesses of 1.5 and 2 nm with surface roughness of ~0.6 and 1 nm, respectively. The larger-than-expected thickness of the samples might be due to disordered regions and polymer residues.

2.2. UPS analysis

The work function of the graphene films was measured by Ultraviolet Photoelectron Spectroscopy (UPS) over a sample area of 1000 μm^2. In a previous work from our group, [40,41] the work function of graphene samples grown at 1070 and 790 °C (transferred on glass/ITO substrates) were evaluated by Kelvin Probe (KP) method, finding values of 4.6 and 4.9 eV, respectively. We then noticed that the work function tended to increase when lowering the growth temperature. Here, we implemented a specific setup and procedure to minimize any contamination (see Methods) and study the work function of our GERS substrates minimizing potential contamination and artifacts. In Fig. 2**,** we show the secondary energy cut off (SECO) of the different as grown samples under He I illumination (21.2 eV). The SECO trend follows that resulting from the KP experiments performed after graphene transfer [40]. Concerning the numerical value of the work functions, 3.9 eV for Gr1070 and 4.5 eV for Gr700, it should be considered that the interaction with copper, and with metal surfaces in general, can effectively dope graphene and significantly shift its work function [42]. Anyhow, from the measurements reported in Fig. 2 it is realistic to presume that Gr700 has a different electronic structure and a higher work function than Gr1070, also after transfer on SiO_2.

2.3. CVD graphene films as SERS substrates

We performed Raman spectroscopy on R6G as a probe molecule. R6G was deposited on the substrates via dip coating (as described in the

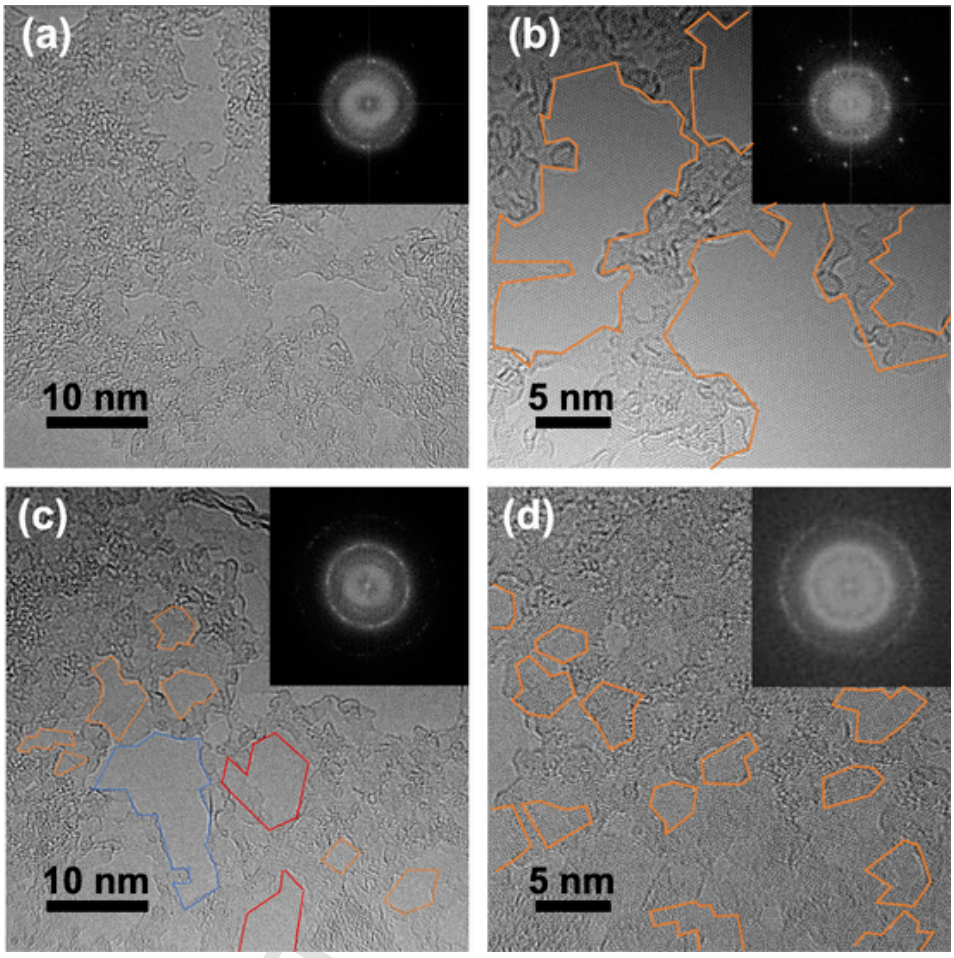

Fig. 1. HRTEM images of Gr860 (a, b), and Gr700 (c, d). The graphene films are composed of highly crystalline grains surrounded by disordered regions. The crystalline grain size decreases as the growth temperature decreases. Inset: FFT images of the corresponding TEM images. Crystalline grains are highlighted by the orange lines in panel b, c and d. The average size of the grains in Gr700 is slightly above ~5 nm; however, a few larger grains were also observed and marked by red lines. The largest area marked in blue identifies a tear in the film, likely due to the transfer process. (For interpretation of the references to colour in this figure legend, the reader is referred to the web version of this article.)

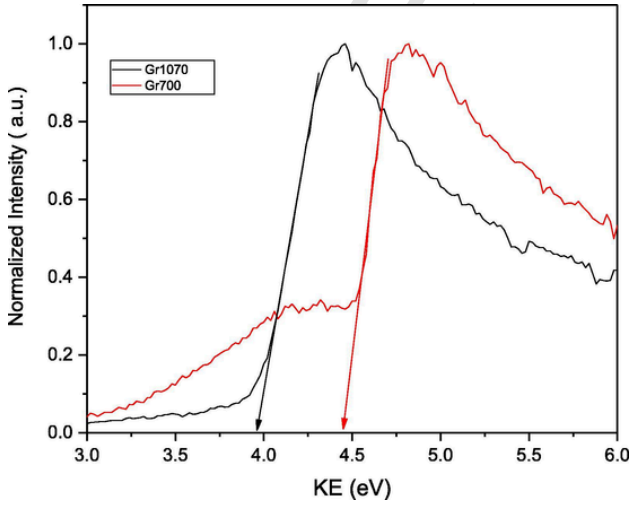

Fig. 2. SECO of the Gr1070 an Gr700 as grown on copper.

Experimental section), which guaranteed a uniform coverage over the entire surface. Typical resonant Raman signals of R6G (6×10^{-5} M) adsorbed on graphene films and on a bare Si/SiO_2 substrate are displayed in **Figure S3a**. When the R6G molecules are deposited on Si/SiO_2 substrate (purple line) no Raman is detected but only a strong PL signal appears. On the graphene films, instead, the PL intensity centered at ≈ 610 cm^{-1} (2.26 eV) decreases and the Raman peaks of R6G appear. The differences in PL emission intensity among the various graphene films and the Si/SiO_2 substrate is attributed to the graphene-induced PL quenching, as previously reported [43,44]. Pristine graphene [11], graphene oxide [45] and graphene-based derivatives [36,46–48] have been widely used as substrates to drastically quench the PL background and enhance the Raman signal from fluorescent molecules, allowing their detection at low concentrations [17]. Dye molecules, as R6G, are characterized by a large fluorescence background, which extends over the entire visible range [49] and hides the Raman signal [17,50]. In **Figure S3b, a** selected region of the spectrum is displayed to highlight the Raman peaks of the R6G/Gr700, whose assignment is in agreement with earlier studies (see **SI**) [51,52]. The comparison with the spectrum of bare Gr700 (black line) shows that the typical D and G bands of graphene materials (1343 and 1595 cm^{-1}, respectively) overlap with the Raman signal of R6G.

The Raman spectra of R6G on the CVD graphene films grown at different temperature are reported in Fig. 3**a** over a selected range. At a first glance, the R6G peaks of R6G/Gr1070 have much lower intensity than the peaks of the other samples. To quantify these observations, Raman enhancement factors (EF) were calculated as the ratio between the R6G SERS signal (*i.e.,* the R6G Raman peaks intensity measured on the GERS substrate) and the R6G Raman signal (measured on bare SiO_2/Si substrate). Details on the EF calculation process are reported in SI [7,

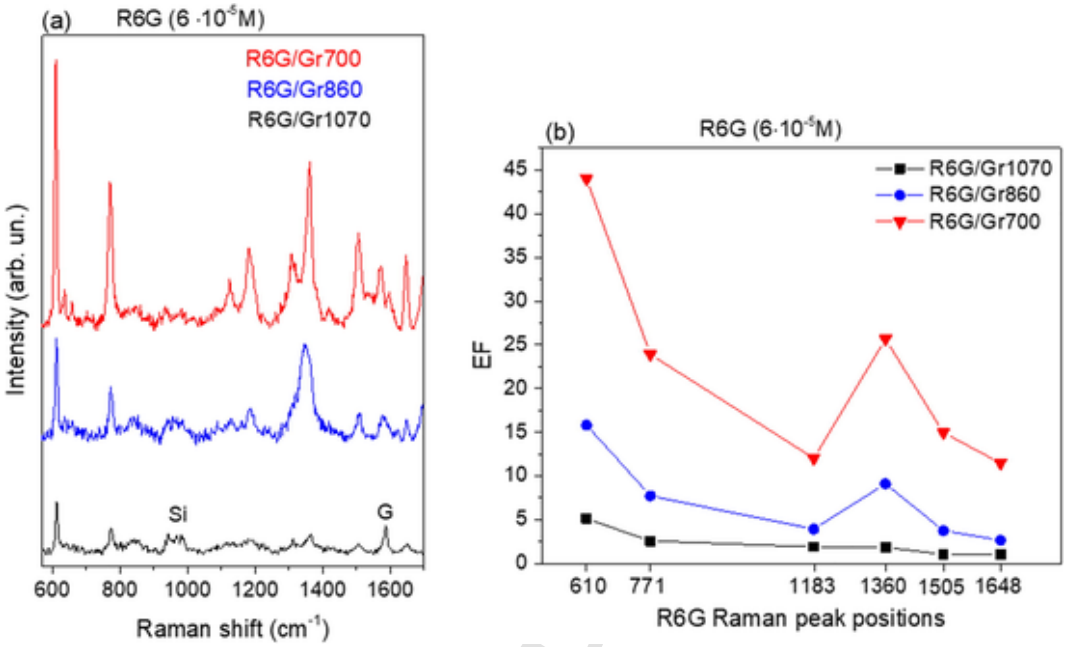

Fig. 3. a) Comparison of the Raman spectra of R6G ($6{\cdot}10^{-5}$ M) on the different graphene films after PL background subtraction. The Spectra were offset for clarity. The peak labelled with "Si" corresponds to the second order Raman Scattering of the silicon substrate b) Enhancement factors for the different R6G Raman peaks calculated from Fig. 3a.

11,23,26]. We focused on six of the characteristic R6G Raman peaks (located at 610 cm^{-1}, 771 cm^{-1}, 1180 cm^{-1}, 1360 cm^{-1}, 1505 cm^{-1}, and 1648 cm^{-1}). The EF values are plotted in function of the R6G Raman peak positions in Fig. 3**b**. Here we observe that R6G peaks are greatly enhanced when deposited on Gr700 (red line in Fig. 3**b**) compared to the other substrates, with EFs ranging from 12 to 45. Moreover, we observe that not all the R6G Raman peaks are enhanced in the same way. Fig. 3**b** highlights that the EF is different for different peaks and that the peak at 610 cm^{-1}, which arises from the C–C–C ring in-plane bending vibration [51], is enhanced the most. Such vibration dependence of the EF is not surprising. It has been reported that the enhancement of different vibrational modes depends on the geometry of the molecule on graphene and is related to the chemical enhancement mechanism [9,11]. At the same time, at 1360 cm^{-1} the enhancement may be influenced by presence of the D line of graphene (see Fig. 3**b**). The uniformity of our samples has been verified by performing Raman mapping. Representative Raman maps of R6G ($6{\cdot}10^{-5}$ M) on Gr700 is reported in SI (**Figure S4**). To confirm the GERS sensitivity of the Gr700 substrate, different organic fluorescent molecules, such as Crystal Violet (CV) and Methylene Blue (MB), were used. The Raman peaks of CV and MB were detected at a concentration of $6{\cdot}10^{-5}$ M, confirming the versatility of the nanocrystalline graphene for molecular sensing (**Figure S5**).

In order to determine the detection limit of our GERS substrates, we performed a systematic investigation by gradually decreasing the concentration of the R6G solution from $6 \cdot 10^{-5}$ to $6 \cdot 10^{-12}$ M. This is the typical concentration range in standard SERS experiments [11]. Fig. 4 shows a comparison between the R6G Raman signal acquired for every molar concentration on Gr1070 (panel a), as standard CVD graphene film, and on the Gr700 substrate (panel b), being the one that gave the best EF results. For both substrates the signal intensity follows the decrease of the dipping solutions concentration. For Gr1070, the detection limit was found when the R6G concentration is $6 \cdot 10^{-9}$ M (Fig. 4**a**), which implies a sub-monolayer coverage of the substrates.[11] The detection limit further improves when R6G molecules are adsorbed on Gr700 (Fig. 4**b**), where well defined R6G Raman peaks can be detected even for a concentration of $6 \cdot 10^{-11}$ M. To the best of our knowledge, this is the first time that a non-doped CVD graphene substrate is used to detect molecules at such low concentrations ($6 \cdot 10^{-9}$ M and $6 \cdot 10^{-11}$ M). Fig. 5**a, b** reports two bar charts summarizing the enhancement factors calculated for the main R6G Raman peaks of the two CVD graphene substrates at the R6G concentration of 6×10^{-9} M and of $6 \cdot 10^{-11}$ M. We can observe that the Gr700 substrate not only enhances the R6G Raman signals with EF values up to 5 times greater compared to Gr1070 at a concentration of 10^{-9} M (panel a), but it also allows to detect molecules at concentrations of 10^{-11} M with remarkable enhancement factors (ranging from 2 to 9), while no R6G Raman signal is detected on Gr1070 (panel b). The EF values calculated for the R6G Raman peaks on Gr860 ranges between a minimum of 0.5 and maximum of 4 at the R6G concentration of $6{\cdot}10^{-9}$ M. No R6G Raman signal is detected on Gr860 at the concentration of $6{\cdot}10^{-11}$M, as shown in **Figure S6 and Figure S7**.

2.4. Role of the nanocrystalline grain size on the GERS effect

Within the aim of describing the electronic interaction of R6G with the nanocrystalline graphene films, we carried out theoretical calculations based on the density functional theory (DFT). In line with the direct HR-TEM observations, we have modelled the nano-sized graphene grains (NGs) by hexagonal clusters, with diameters of 1.2, 1.7, 2.7 and 3.7 nm, passivated by hydrogen on the edges, as shown in Fig. 6**a**. The graphene has been modelled by using a periodic supercell (Fig. 6**b**). The model of R6G takes into account the interaction with the Cl^- counter-ion. We found that the role of the counter-ion is important since the highest occupied molecular orbital (HOMO) level is localized on it (Fig. 7).

The difference between the lowest unoccupied molecular orbital (LUMO) and the HOMO energy levels for R6G calculated with the correlation functional Perdew, Burke and Ernzerhof (PBE) is found to be 0.76 eV, while the estimation of the hybrid correlation functional PBE0, more accurate than PBE, is 2.3 eV, in good agreement with the R6G absorption maximum (approximately 530 nm). The model in which R6G molecule is passivated with hydrogen (no counter-ion) gives a different HOMO level and a PBE0 energy gap of 2.99 eV, which is much higher compared to the experimental results. Liu and co-authors [35] used this last model to describe the interaction of R6G with graphene and GQDs

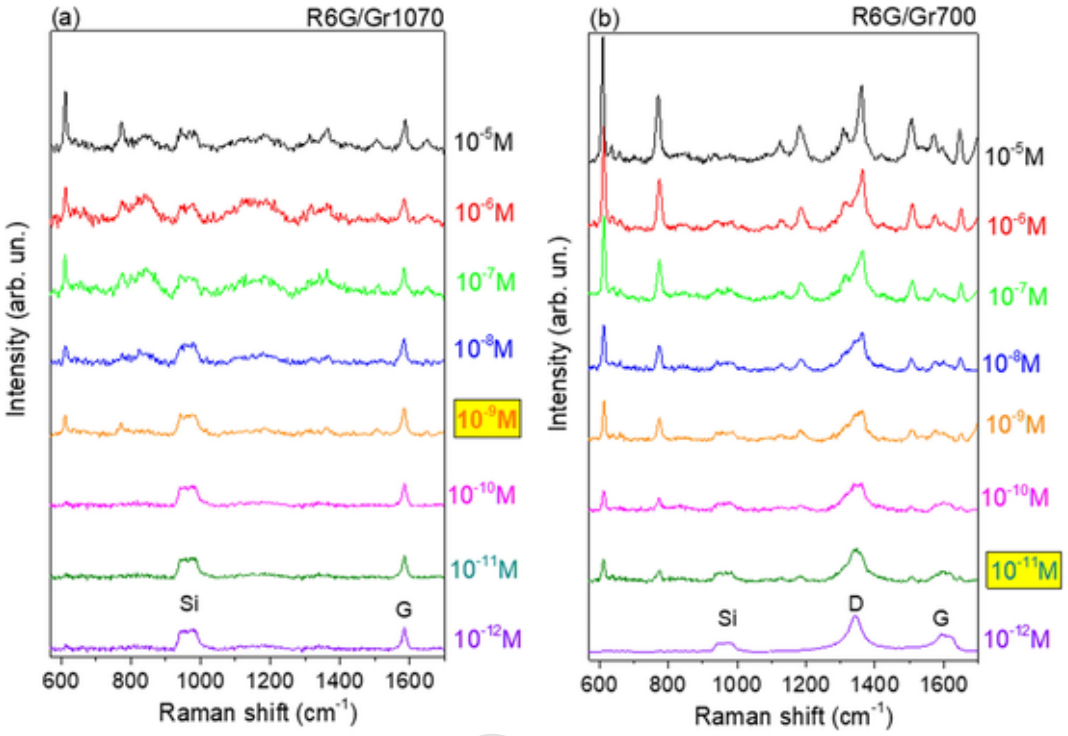

Fig. 4. Raman spectra of R6G deposited on Gr1070 (a), Gr700 (b). The R6G concentration was gradually decreased from $6{\cdot}10^{-5}$ to $6{\cdot}10^{-12}$ M. The detection limit of each substrate is marked in yellow. The peak labelled with "Si" corresponds to the second order Raman Scattering of the silicon substrate. (For interpretation of the references to colour in this figure legend, the reader is referred to the web version of this article.)

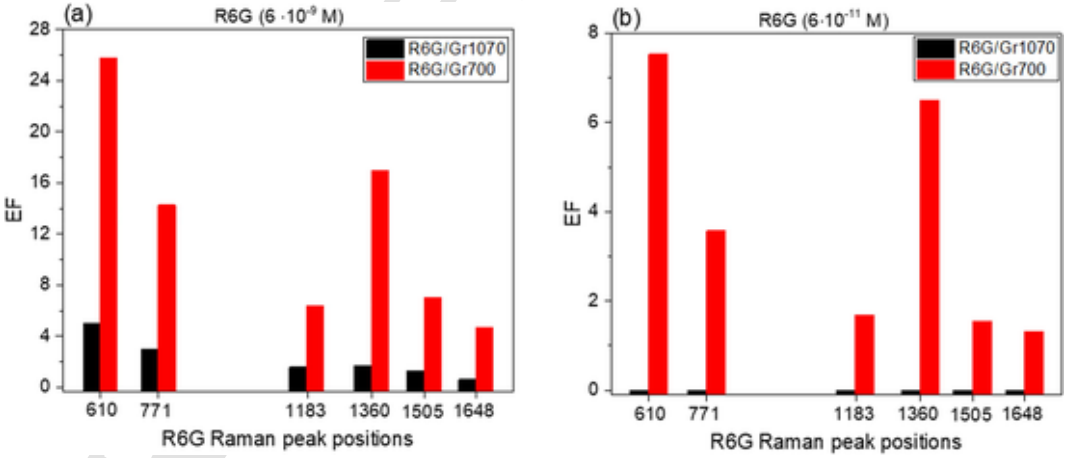

Fig. 5. Bar chart summarizing the EFs of the Raman signals of R6G molecules at concentrations of $6 \cdot 10^{-9}$ M (a) and $6 \cdot 10^{-11}$M (b) for both graphene substrates. No R6G Raman signal is detected on Gr1070 at the concentration of $6{\cdot}10^{-11}$M.

used as GERS substrates. We improved their model by taking into account the HOMO localization around the Cl^- counter-ion. Fig. 6**c** shows that the R6G HOMO level (solid orange lines) is localized in the NG gap (between the NG HOMO and NG LUMO in black solid and dashed lines, respectively). In other words, the R6G HOMO is not aligned with the NG HOMO (solid black lines). However, we found an increase of the NG HOMO levels with the increase of the grains size (Fig. 6**c**), leading to a reduction of the energy difference between the R6G and NG HOMOs (ΔH) for large clusters. Our calculations demonstrate that the R6G/NG systems (with NG size < 3.7 nm) do not achieve an alignment of the HOMO levels such as to favor an efficient ground-state charge transfer. [11,24] In contrast, when R6G molecule is adsorbed in the periodic supercell of graphene, the R6G HOMO level is located below the graphene Fermi level (Fig. 6**d and Figure S8**) favoring the charge transfer. Thus, if we consider the graphene Fermi level as the HOMO level of a NG of infinite diameter, we can conclude that a NG critical diameter must exist that allows the most effective ground-state charge transfer. We estimate such critical diameter to be in the range 5–7 nm by fitting the calculated data. Indeed, we have found significant correlation for the exponential decay of the NGs energy gap and ΔH. In this way, we can extrapolate the NG size corresponding to the perfect energy level alignment ($\Delta H = 0$) in the above-mentioned range (**Figure S9**).

3. Discussion

As mentioned in the introduction, the GERS originates exclusively from a chemical enhancement mechanism [18], a short-range effect based on a ground-state charge transfer between the molecules and the substrate [18]. Two requirements must be met for a charge transfer to occur: i) a distance between molecule and substrate below 0.2 nm

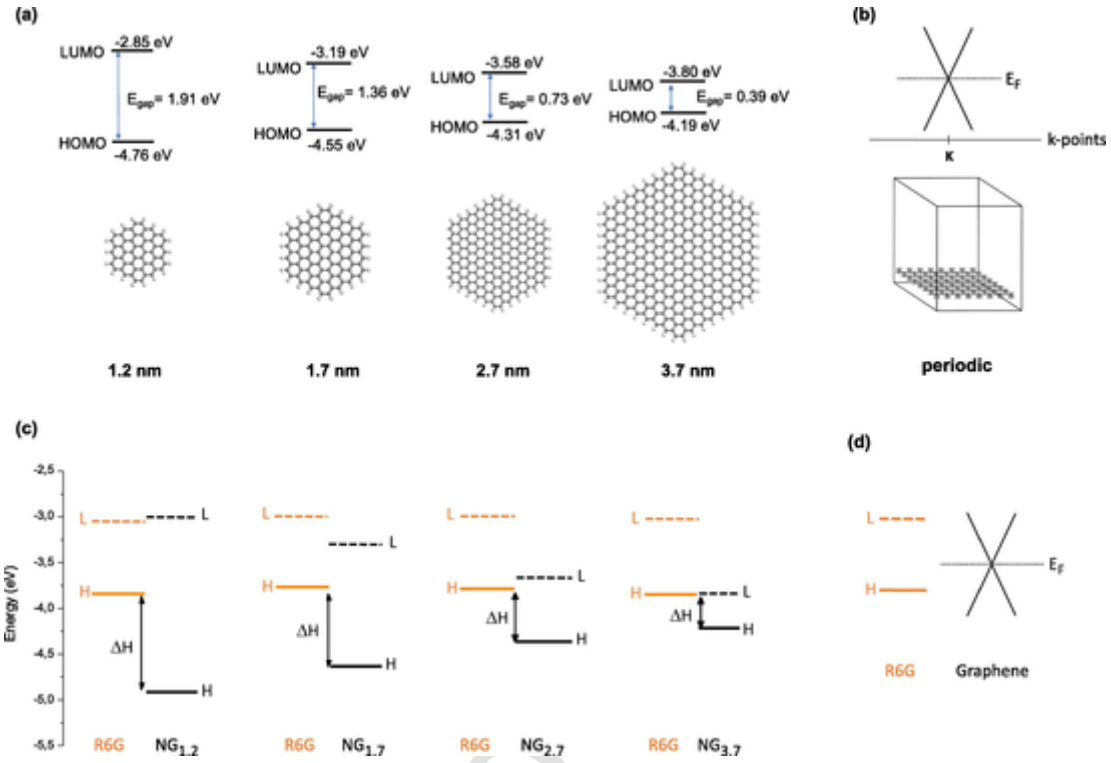

Fig. 6. (a) Atomistic models of the NG grains with diameters of 1.2, 1.7, 2.7 and 3.7 nm. The corresponding HOMO and LUMO energy levels as well the energy gap E_{gap} are shown above each structure. C and H atoms are grey and white, respectively. (b) graphene periodic supercell model and band structure; (c) energy levels of the R6G/NG model for diameters of 1.2 nm ($NG_{1.2}$), 1.7 nm ($NG_{1.7}$), 2.7 nm ($NG_{2.7}$) and 3.7 nm ($NG_{3.7}$). The energy difference between the R6G HOMO and the NG HOMO levels (ΔH) are: 1.07 eV ($NG_{1.2}$), 0.87 eV ($NG_{1.7}$), 0.58 eV ($NG_{2.7}$), and 0.37 eV ($NG_{3.7}$). (d) Energy level diagram of R6G/graphene system. The R6G HOMO level is located 0.25 eV below the graphene Fermi level.

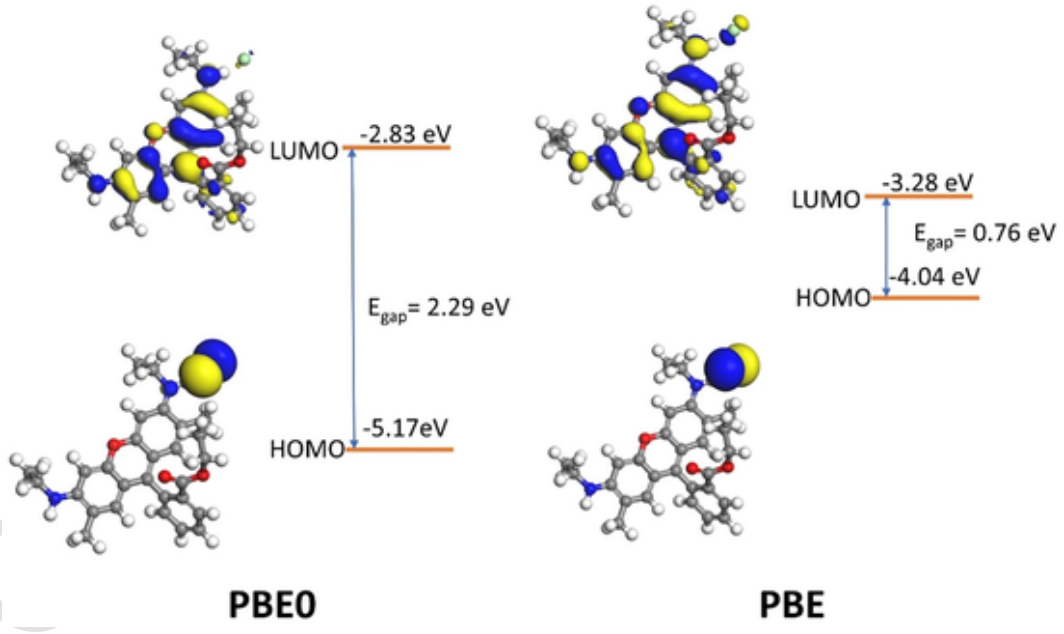

Fig. 7. HOMO, LUMO and energy levels of R6G calculated with PBE0 (on the left) and PBE (on the right) correlation functional. C, O, H and Cl atoms are grey, red, white and green, respectively. (For interpretation of the references to colour in this figure legend, the reader is referred to the web version of this article.)

(first-layer effect) and ii) a match between the energy levels of molecule and substrate [12]. More specifically, if we consider the R6G/graphene system (Fig. 6**d**), the Fermi level position with respect to the R6G HOMO allows the electrons of graphene to contribute to the Raman scattering. The shorter the distance between those two energy levels, the more efficient will be the charge transfer [53].

Our results demonstrate that nanocrystalline CVD graphene can act as highly efficient GERS substrate. At the R6G concentration of 10^{-5} M, the EFs measured for the nanocrystalline graphene films (Gr860 and Gr700) were found to be 3 to 9 times higher than that measured on high quality monolayer graphene (Gr1070) (Fig. 3**b**). Moreover, Gr700 substrate has shown high sensitivity for all the R6G concentrations and the

ability to detect molecules down to 6 × 10^{-11} M (Fig. 5**b**). An experimental explanation is given by the UPS results (Fig. 2): When moving from pristine to nanocrystalline graphene, the electronic structure changes and the work function increases, thus establishing a closer matching with the HOMO level of R6G. Furthermore, by modelling the atomic structure of film (made of sp^2 nano-grains of different size embedded in a disorder carbon matrix), a dependence of the Raman enhancement on the grain size emerges, possibly hinting at a role of grain boundaries and defects too. We found that a critical NG diameter exists that allows the R6G and NG HOMO levels to be aligned. In the case of R6G/Gr700 system, most of crystalline grains have a size in the range of 5–7 nm (Fig. 1**d**) that, according to the DFT calculations, corresponds to the highest ground-state charge transfer efficiency. Moreover, compared to crystalline graphene film (Gr1070), nanocrystalline graphene films (Gr700) have more edges and thus, under the same R6G concentration, a more effective adsorption of molecules may occur. At ultra-low concentrations (10^{-9} M and 10^{-11} M), for which the number of molecules is very low, the role played by the edge is further confirmed and quantified in **Figure S10** at the R6G concentration of 6 × 10^{-9} M, where R6G/Gr700 system show a twice higher PL background compared to R6G/Gr1070 one. Nevertheless, the increased number of molecules is not enough to justify the full extent of the measured EFs (an increase by a factor five) shown in Fig. 5**a**.

4. Conclusion

We developed an ultrasensitive GERS substrate, consisting in a large-area CVD graphene film composed of nanocrystalline grains embedded in an amorphous carbon matrix. Raman enhancement experiments have shown the high efficiency of our GERS substrate (referred as Gr700), which is able to detect R6G molecules down to 10^{-11} M. To the best of our knowledge, such detection limit has never achieved before with a non-doped CVD graphene film. UPS measurements revealed that Gr700 work function increased with respect to that measured for a standard high-quality CVD graphene film, demonstrating a modification in the electronic structure of the nanocrystalline film. Such results are in line with the DFT calculations, performed by modeling the nano-sized graphene grains as hexagonal clusters, and the standard graphene as a periodic supercell. The increased work function results in a better energy matching between the R6G and the NGs HOMO levels, allowing the involvement of more electrons in the Raman scattering and consequently a larger enhancement effect in the R6G/Gr700 system. The synergistic action of the direct contact between the molecule and the substrate, the energy alignment between the R6G the NGs HOMOs, together with the abundance of grains edges able to adsorb in increased number of molecules, appear to favor an extremely high sensitivity of our GERS substrate. Although femtomolar detection limits for R6G molecules have been achieved by using 2D materials based on transition-metal dichalcogenides, our results are the best obtained for as grown graphene and derivatives, not combined in heterostructure. Overall, we have demonstrated that a nanocrystalline CVD graphene film, easily transferrable onto arbitrary surfaces, represents a significant advancement in the nano-engineering of SERS platforms, especially for biological applications.

5. Experimental and theoretical methods

5.1. Growth and transfer of graphene-based films

Graphene was grown by CVD process as previously described [54]. A copper foils with a thickness of 25 μm (Aldrich) was used. After loading of a cleaned copper foil, the temperature was increased to a desired value (700, 860 and 1070 °C). Before growth, a mixture of Ar and H_2 (20 : 20 SCCM) was inserted, then a mixture of Ar, H_2, and ethanol was provided (Ar : H_2 : ethanol = 15 : 10 : 0.1 SCCM at 1070 °C for FLG, Ar : H_2 : ethanol = 15 : 10 : 0.02 SCCM at 1070 °C for SLG, Ar : ethanol = 15 : 0.1 SCCM at 700 °C for nanocrystalline graphene). After growth the samples can be either rapidly mounted onto a specially designed support and inserted in ultra-high vacuum UPS pre-chamber for the determination of the WF (few minutes exposure to air), or transferred onto other substrates for processing and application. Transfer of the TEM samples was performed through the IPA method [55] directly on TEM grids. Samples for Raman and GERS studies are transferred onto Si/SiO_2 (300 nm) using a temporary cyclododecane [56] layer to protect graphene during the etching of copper in an Ammonium Persulfate solution (60 g/l) at 4 °C for a few hours. After rinsing in abundant distilled water, the samples are scooped directly with the target substrates and heated to 60 °C to remove the cyclododecane and finally cleaned in Ethyl Acetate vapor.

5.2. Work function measurements via UPS

Since work function measurements are extremely sensitive to surface contaminants and processing, we performed the measurements in a controlled UPS experimental setup. The Cu foil substrate were precut to the required 12 mm diameter disk size before growth. Immediately after extraction from the CVD at room temperature under inert gas, the disks were placed onto UPS sample holders, inserted in the system high vacuum pre-chamber and pumped down to 10^{-8} mbar in a few minutes. To the best of our knowledge, there are very few reports in the literature for work function measurements of graphene on copper [57], if any in the case of just-grown graphene or of graphene inserted in UPS chamber via load locks. Overall this procedure granted minimal contamination. The work function was measured from the secondary energy cut off (SECO), taking into account the position of the Fermi Edge, under He I illumination at 21.2 eV under −6 V sample bias, in a Vacuum Science ESCALAB MKII. The sample holder design and analyzer apertures were carefully set to gather reproducible results [58].

5.3. R6G deposition on graphene-based substrates

R6G molecules were deposited on the surface of the graphene substrates via dip coating method by using a series of R6G solutions of known concentrations. R6G (Sigma-Aldrich) was first dissolved in distilled water with a concentration of 6 × 10^{-5} M and then progressively diluted in the same solvent, obtaining 7 new concentrations: 6 × 10^{-6}, 6 × 10^{-7}, 6 × 10^{-8}, 6 × 10^{-9}, 6 × 10^{-10}, 6 × 10^{-11} and 6 × 10^{-12} M. The substrates were dipped in each solution for 2 h30 and then rinsed with distilled water to remove the excess of R6G molecules, before being dried under nitrogen flow.

5.4. Micro-Raman/PL spectroscopy

Micro-Raman/PL measurements were performed by means of a HORIBA Scientific LabRAM HR Evolution Raman spectrometer with an integrated Olympus BX41 microscope using a 600 lines/mm grating and a 100x objective. A laser excitation wavelength of 532 nm was focused on the surface with a spot size of approximately 0.7 μm in diameter. Low laser power of 0.65 mW and an integration time of 1 s were chosen to minimize the heating effect induced by laser. All spectra were recorded at room temperature. Raman measurements were made in a minimum of ten different points of each sample in order to account for homogeneities. Where necessary the fluorescence background was subtracted by applying a polynominal fit using the LabSpec software from Horiba.

5.5. TEM imaging

The carbon layer grown on the back of the Cu foil was removed by O_2 plasma cleaning (O_2 plasma condition: 20 sccm/100 W/5 min/

100 kHz, Femto Science). Graphene was directly transferred to a TEM grid to minimize potential residues [55]. The Cu foil was etched by ammonium persulfate (20 wt%) for 2 h, followed by rinsing in DI water. For structural characterization, we used TEM (JEOL, JEM-ARM 200F) with low operating voltage of 80 kV to minimize any radiation damage of the graphene samples.

5.6. AFM imaging

Amplitude modulation AFM (AM – AFM) micrographs were acquired in air using an AIST-NT SmartSPM working in tapping mode. The microscope is equipped with a scanning head providing a maximum image range of 100 × 100 μm, a conventional piezoscanner (maximum xy range 100 μm and maximum z range 15 μm) and a four-segment photodetector for cantilever deflection monitoring. A camera and an optical microscope with a 100x objective lens allow precise tip positioning. High quality AFM probes from MikroMasch (cantilever length: 125 μm; nominal spring constant: 5 N/m) were used with Al backside reflex coating, a resonance frequency of ~160 kHz and a tip apical radius of 8 nm. Measurements were performed by scanning a minimum of five different areas for each sample. For each area, at least 10 sites were scanned. The scan rate and the oscillation amplitude were set to 0,5 Hz and 20 nm, respectively. All the scans were acquired at room temperature. The collected data were postprocessed using AIST-NT image processing software. The AFM topography images were plane corrected and the noise was removed by subtracting the mean value from each scan line. Surface roughness values was calculated by averaging the values acquired from at least five different regions for each sample.

5.7. DFT calculations

The theoretical investigation was carried out with calculations based on the density functional theory (DFT) within the generalized gradient approximation (GGA) with the Perdew, Burke and Ernzerhof (PBE) correlation functional [59]. We used also the more accurate but more computationally demanding PBE0 hybrid correlation functional [60] in order to compare the results for the isolated R6G molecule with those obtained using the PBE correlation. Our calculations were performed using the DMol^3 program [61,62] available as a part of the Materials Studio software [63]. The electronic wavefunctions are expanded in atom-centered basis functions defined on a dense numerical grid. The chosen basis set was DNP (double numerical plus polarization) where each basis function was restricted to a global cut-off radius of 4.5 Å. The chosen cut-off value leads to atomic energies with an accuracy of 0.1 eV/atom, allowing calculations without a significant loss of accuracy. All geometry optimizations were performed using a scheme based on delocalized internal coordinates. We set the geometry optimization convergence thresholds for energy change, maximum force, and maximum displacement to 10^{-5} Hartree, 0.002 Hartree/Å and 0.001 Å, respectively. We have modeled the graphene clusters with the $C_{96}H_{24}$, $C_{216}H_{36}$ and $C_{384}H_{48}$ hexagonal clusters passivated by Hydrogen on the edges, with diameter of 1.2, 1.7, 2.7 and 3.7 nm, respectively. The graphene has been modelled by using 8 × 8 supercell and imposing periodic boundary conditions. The width of the vacuum in the direction perpendicular to the graphene plane is such that the interactions among the periodic images of the system are negligible. We verified negligible interactions among the R6G molecule and its periodic images, as well.

Uncited reference

[15].

CRediT authorship contribution statement

Giuliana Faggio: Conceptualization, Validation, Investigation, Writing – original draft, Resources. **Rossella Grillo:** Conceptualization, Investigation, Writing – original draft. **Nicola Lisi:** Conceptualization, Investigation, Writing – review & editing. **Francesco Buonocore:** Formal analysis, Software. **Rosa Chierchia:** Investigation. **Min Jung Kim:** Investigation. **Gwan-Hyoung Lee:** Investigation, Resources. **Andrea Capasso:** Conceptualization, Writing – review & editing. **Giacomo Messina:** Conceptualization, Writing – review & editing, Resources, Supervision.

Declaration of Competing Interest

The authors declare that they have no known competing financial interests or personal relationships that could have appeared to influence the work reported in this paper.

Acknowledgements

This publication is co-financed with the support of the European Commission, the European Social Fund, and the Calabria Region (CUP: C31J19000010002).

G.H.L acknowledges the supports from Basic Science Research Program and the International Research & Development Program through the NRF of Korea (2019K1A3A1A25000267, NRF-2021R1A2C3014316) and Creative-Pioneering Researchers Program through Seoul National University (SNU).

A.C. acknowledges the financial support of the project "GEMIS – Graphene-enhanced Electro Magnetic Interference Shielding" with the reference POCI-01-0247-FEDER-045939, co-funded by COMPETE 2020 – Operational Programme for Competitiveness and Internationalization and FCT –Science and Technology Foundation, under the Portugal 2020 Partnership Agreement, through the European Regional Development Fund (ERDF).

The computing resources and the related technical support used for this work have been provided by CRESCO/ENEAGRID High Performance Computing infrastructure and its staff. CRESCO/ENEAGRID High Performance Computing infrastructure is funded by ENEA, the Italian National Agency for New Technologies, Energy and Sustainable Economic Development and by Italian and European research programs, see http://www.cresco.enea.it/english for information.

Appendix A. Supplementary data

Supporting Information are available: Rhodamine 6G (R6G) Raman signal, Enhancement Factor calculation, Raman Spectra of the Graphene films, AFM Imaging, calculated HOMO, LUMO and energy levels of R6G. Supplementary data to this article can be found online at https://doi.org/10.1016/j.apsusc.2022.154035.

References

[1] A. Campion, P. Kambhampati, Surface-Enhanced Raman Scattering, Chem. Soc. Rev. 27 (4) (1998) 241, https://doi.org/10.1039/a827241z.
[2] M. Moskovits, Surface-Enhanced Raman Spectroscopy: A Brief Retrospective, J. Raman Spectrosc. 36 (6–7) (2005) 485–496, https://doi.org/10.1002/jrs.1362.
[3] P.G. Etchegoin, E.C. Ru Le, A Perspective on Single Molecule SERS: Current Status and Future Challenges, Phys. Chem. Chem. Phys. 10 (40) (2008) 6079–6089, https://doi.org/10.1039/B809196J.
[4] S. Nie, S.R. Emory, Probing Single Molecules and Single Nanoparticles by Surface-Enhanced Raman Scattering, Science (80-.) 275 (5303) (1997) 1102–1106.
[5] K. Kneipp, Y. Wang, H. Kneipp, L.T. Perelman, I. Itzkan, R.R. Dasari, M.S. Feld, Single Molecule Detection Using Surface-Enhanced Raman Scattering (SERS), Phys. Rev. Lett. 78 (9) (1997) 1667–1670, https://doi.org/10.1103/PhysRevLett.78.1667.
[6] P.L. Stiles, J.A. Dieringer, N.C. Shah, R.P. Van Duyne, Surface-Enhanced Raman Spectroscopy, Annu. Rev. Anal. Chem. 1 (1) (2008) 601–626.

[7] A. Foti, C. D'Andrea, F. Bonaccorso, M. Lanza, G. Calogero, E. Messina, O.M. Maragò, B. Fazio, P.G. Gucciardi, A Shape-Engineered Surface-Enhanced Raman Scattering Optical Fiber Sensor Working from the Visible to the Near-Infrared, Plasmonics 8 (1) (2013) 13–23, https://doi.org/10.1007/s11468-012-9371-3.

[8] M.I. Stockman, Electromagnetic Theory of SERS, Surface-Enhanced Raman Scatt. (2006) 47–65, https://doi.org/10.1007/3-540-33567-6_3.

[9] A. Otto, The, "chemical" (Electronic) Contribution to Surface-Enhanced Raman Scattering, J. Raman Spectrosc. 36 (6–7) (2005) 497–509, https://doi.org/10.1002/jrs.1355.

[10] G.C. Schatz, M.A. Young, R.P. Duyne, Electromagnetic Mechanism of SERS, Surface-Enhanced Raman Scatt. (2006) 19–45, https://doi.org/10.1007/3-540-33567-6_2.

[11] X. Ling, L. Xie, Y. Fang, H. Xu, H. Zhang, J. Kong, M.S. Dresselhaus, J. Zhang, Z. Liu, Can Graphene Be Used as a Substrate for Raman Enhancement? Nano Lett. 10 (2) (2010) 553–561, https://doi.org/10.1021/nl903414x.

[12] W. Xu, N. Mao, J. Zhang, Graphene: A Platform for Surface-Enhanced Raman Spectroscopy, Small 9 (8) (2013) 1206–1224, https://doi.org/10.1002/smll.201203097.

[13] X. Ling, J. Zhang, First-Layer Effect in Graphene-Enhanced Raman Scattering, Small 6 (18) (2010) 2020–2025, https://doi.org/10.1002/smll.201000918.

[14] B. Sharma, R.R. Frontiera, A.I. Henry, E. Ringe, R.P. Van Duyne, SERS: Materials, Applications, and the Future, Mater. Today 15 (1–2) (2012) 16–25, https://doi.org/10.1016/S1369-7021(12)70017-2.

[15] M. Liu, H. Zhao, X. Quan, S. Chen, X. Fan, Distance-Independent Quenching of Quantum Dots by Nanoscale-Graphene in Self-Assembled Sandwich Immunoassay, Chem. Commun. 46 (42) (2010) 7909, https://doi.org/10.1039/c0cc02085k.

[16] N. Zhang, L. Tong, J. Zhang, Graphene-Based Enhanced Raman Scattering toward Analytical Applications, Chem. Mater. 28 (18) (2016) 6426–6435, https://doi.org/10.1021/acs.chemmater.6b02925.

[17] L. Xie, X. Ling, Y. Fang, J. Zhang, Z. Liu, Graphene as a Substrate to Suppress Fluorescence in Resonance Raman Spectroscopy, J. Am. Chem. Soc. 131 (29) (2009) 9890–9891, https://doi.org/10.1021/ja9037593.

[18] X. Ling, L.G. Moura, M.A. Pimenta, J. Zhang, Charge-Transfer Mechanism in Graphene-Enhanced Raman Scattering, J. Phys. Chem. C 116 (47) (2012) 25112–25118, https://doi.org/10.1021/jp3088447.

[19] R.A. Tripp, R.A. Dluhy, Y. Zhao, Novel Nanostructures for SERS Biosensing, Nano Today 3 (3–4) (2008) 31–37, https://doi.org/10.1016/S1748-0132(08)70042-2.

[20] Z. Liu, J.T. Robinson, X. Sun, H. Dai, PEGylated Nanographene Oxide for Delivery of Water-Insoluble Cancer Drugs, J. Am. Chem. Soc. 130 (33) (2008) 10876–10877, https://doi.org/10.1021/ja803688x.

[21] Y. Chen, H. Liu, J. Jiang, C. Gu, Z. Zhao, T. Jiang, Immunoassay of Tumor Markers Based on Graphene Surface-Enhanced Raman Spectroscopy, ACS Appl. Bio Mater. 3 (11) (2020) 8012–8022, https://doi.org/10.1021/acsabm.0c0109810.1021/acsabm.0c01098.s001.

[22] X.i. Ling, J. Wu, L. Xie, J. Zhang, Graphene-Thickness-Dependent Graphene-Enhanced Raman Scattering, J. Phys. Chem. C 117 (5) (2013) 2369–2376.

[23] S. Huang, X. Ling, L. Liang, Y. Song, W. Fang, J. Zhang, J. Kong, V. Meunier, M.S. Dresselhaus, Molecular Selectivity of Graphene-Enhanced Raman Scattering, Nano Lett. 15 (5) (2015) 2892–2901, https://doi.org/10.1021/nl5045988.

[24] E.B. Barros, M.S. Dresselhaus, Theory of Raman Enhancement by Two-Dimensional Materials: Applications for Graphene-Enhanced Raman Spectroscopy, Phys. Rev. B - Condens. Matter Mater. Phys. 90 (3) (2014), https://doi.org/10.1103/PhysRevB.90.035443.

[25] S. Feng, M.C. dos Santos, B.R. Carvalho, R. Lv, Q. Li, K. Fujisawa, A.L. Elías, Y.u. Lei, N. Perea-López, M. Endo, M. Pan, M.A. Pimenta, M. Terrones, Ultrasensitive Molecular Sensor Using N-Doped Graphene through Enhanced Raman Scattering, Sci. Adv. 2 (7) (2016), https://doi.org/10.1126/sciadv.1600322.

[26] J. Seo, J. Lee, Y. Kim, D. Koo, G. Lee, H. Park, Ultrasensitive Plasmon-Free Surface-Enhanced Raman Spectroscopy with Femtomolar Detection Limit from 2D van Der Waals Heterostructure, Nano Lett. 20 (3) (2020) 1620–1630, https://doi.org/10.1021/acs.nanolett.9b0464510.1021/acs.nanolett.9b04645.s001.

[27] Q. Lv, X. Wu, J. Tan, B. Liu, L. Gan, J. Li, Z.H. Huang, F. Kang, R. Lv, Ultrasensitive Molecular Sensing of Few-Layer Niobium Diselenide, J. Mater. Chem. A 9 (5) (2021) 2725–2733, https://doi.org/10.1039/d0ta09520f.

[28] X. Song, Y. Wang, F. Zhao, Q. Li, H.Q. Ta, M.H. Rümmeli, C.G. Tully, Z. Li, W.-J. Yin, L. Yang, K.-B. Lee, J. Yang, I. Bozkurt, S. Liu, W. Zhang, M. Chhowalla, Plasmon-Free Surface-Enhanced Raman Spectroscopy Using Metallic 2D Materials, ACS Nano 13 (7) (2019) 8312–8319, https://doi.org/10.1021/acsnano.9b0376110.1021/acsnano.9b03761.s001.

[29] C. Qiu, H. Zhou, H. Yang, M. Chen, Y. Guo, L. Sun, Investigation of N-Layer Graphenes as Substrates for Raman Enhancement of Crystal Violet, J. Phys. Chem. C 115 (20) (2011) 10019–10025, https://doi.org/10.1021/JP111617C.

[30] X. Yu, H. Cai, W. Zhang, X. Li, N. Pan, Y. Luo, X. Wang, J.G. Hou, Tuning Chemical Enhancement of SERS by Controlling the Chemical Reduction of Graphene Oxide Nanosheets, ACS Nano 5 (2) (2011) 952–958, https://doi.org/10.1021/NN102291J.

[31] S. Huh, J. Park, Y.S. Kim, K.S. Kim, B.H. Hong, J.-M. Nam, UV/Ozone-Oxidized Large-Scale Graphene Platform with Large Chemical Enhancement in Surface-Enhanced Raman Scattering, ACS Nano 5 (12) (2011) 9799–9806, https://doi.org/10.1021/NN204156N.

[32] Y. Chen, H. Liu, X. Li, S. Tang, C. Gu, G. Wei, T. Jiang, X. Zhou, Development of RGO@MoS2@Ag Ternary Nanocomposites with Tunable Geometry Structure for Recyclable SERS Detection, Sensors Actuators, B Chem. 339 (March) (2021) 129856, https://doi.org/10.1016/j.snb.2021.129856.

[33] B. Huang, Z. Li, Z. Liu, G. Zhou, S. Hao, J. Wu, B.-L. Gu, W. Duan, Adsorption of Gas Molecules on Graphene Nanoribbons and Its Implication for Nanoscale Molecule Sensor, J. Phys. Chem. C 112 (35) (2008) 13442–13446, https://doi.org/10.1021/JP8021024.

[34] H. Cheng, Y. Zhao, Y. Fan, X. Xie, L. Qu, G. Shi, Graphene-Quantum-Dot Assembled Nanotubes: A New Platform for Efficient Raman Enhancement, ACS Nano 6 (3) (2012) 2237–2244, https://doi.org/10.1021/NN204289T.

[35] D. Liu, X. Chen, Y. Hu, T. Sun, Z. Song, Y. Zheng, Y. Cao, Z. Cai, M. Cao, L. Peng, Y. Huang, L. Du, W. Yang, G. Chen, D. Wei, A.T.S. Wee, D. Wei, Raman Enhancement on Ultra-Clean Graphene Quantum Dots Produced by Quasi-Equilibrium Plasma-Enhanced Chemical Vapor Deposition, Nat. Commun. 9 (1) (2018), https://doi.org/10.1038/s41467-017-02627-5.

[36] J. Liu, H. Cai, X. Yu, K. Zhang, X. Li, J. Li, N. Pan, Q. Shi, Y. Luo, X. Wang, Fabrication of Graphene Nanomesh and Improved Chemical Enhancement for Raman Spectroscopy, J. Phys. Chem. C 116 (29) (2012) 15741–15746, https://doi.org/10.1021/JP303265D.

[37] A. Capasso, J. Rodrigues, M. Moschetta, F. Buonocore, G. Faggio, G. Messina, M.J. Kim, J. Kwon, E. Placidi, F. Benfenati, M. Bramini, G.-H. Lee, N. Lisi, Interactions between Primary Neurons and Graphene Films with Different Structure and Electrical Conductivity, Adv. Funct. Mater. 31 (11) (2021) 2005300, https://doi.org/10.1002/adfm.202005300.

[38] G. Faggio, G. Messina, C. Lofaro, N. Lisi, A. Capasso, Recent Advancements on the CVD of Graphene on Copper from Ethanol Vapor, C — J. Carbon Res. 6 (1) (2020) 14, https://doi.org/10.3390/c6010014.

[39] G. Faggio, A. Capasso, G. Messina, S. Santangelo, T. Dikonimos, S. Gagliardi, R. Giorgi, V. Morandi, L. Ortolani, N. Lisi, High-Temperature Growth of Graphene Films on Copper Foils by Ethanol Chemical Vapor Deposition, J. Phys. Chem. C 117 (41) (2013) 21569–21576, https://doi.org/10.1021/jp407013y.

[40] A. Capasso, L. Salamandra, G. Faggio, T. Dikonimos, F. Buonocore, V. Morandi, L. Ortolani, N. Lisi, Chemical Vapor Deposited Graphene-Based Derivative As High-Performance Hole Transport Material for Organic Photovoltaics, ACS Appl. Mater. Interfaces 8 (36) (2016) 23844–23853, https://doi.org/10.1021/acsami.6b06749.

[41] A. Gnisci, G. Faggio, L. Lancellotti, G. Messina, R. Carotenuto, E. Bobeico, P. Delli Veneri, A. Capasso, T. Dikonimos, N. Lisi, The Role of Graphene-Based Derivative as Interfacial Layer in Graphene/n-Si Schottky Barrier Solar Cells, Phys. Status Solidi Appl. Mater. Sci. 216 (3) (2019) 1800555.

[42] G. Giovannetti, P.A. Khomyakov, G. Brocks, V.M. Karpan, J. Van Den Brink, P.J. Kelly, Doping Graphene with Metal Contacts, Phys. Rev. Lett. 101 (2) (2008) 4–7, https://doi.org/10.1103/PhysRevLett.101.026803.

[43] B. Yang, E. Molina, J. Kim, D. Barroso, M. Lohmann, Y. Liu, Y. Xu, R. Wu, L. Bartels, K. Watanabe, T. Taniguchi, J. Shi, Effect of Distance on Photoluminescence Quenching and Proximity-Induced Spin-Orbit Coupling in Graphene/WSe2 Heterostructures, Nano Lett. 18 (6) (2018) 3580–3585.

[44] A. Kasry, A.A. Ardakani, G.S. Tulevski, B. Menges, M. Copel, L. Vyklicky, Highly Efficient Fluorescence Quenching with Graphene, J. Phys. Chem. C 116 (4) (2012) 2858–2862, https://doi.org/10.1021/JP207972F.

[45] H. Yang, H. Hu, Z. Ni, C.K. Poh, C. Cong, J. Lin, T. Yu, Comparison of Surface-Enhanced Raman Scattering on Graphene Oxide, Reduced Graphene Oxide and Graphene Surfaces, Carbon N. Y. 62 (2013) 422–429, https://doi.org/10.1016/j.carbon.2013.06.027.

[46] Y. Hu, Á.I. López-Lorente, B. Mizaikoff, Graphene-Based Surface Enhanced Vibrational Spectroscopy: Recent Developments, Challenges, and Applications, ACS Photonics 6 (9) (2019) 2182–2197, https://doi.org/10.1021/acsphotonics.9b00645.

[47] X. Ling, S. Huang, S. Deng, N. Mao, J. Kong, M.S. Dresselhaus, J. Zhang, Lighting Up the Raman Signal of Molecules in the Vicinity of Graphene Related Materials, Acc. Chem. Res. 48 (7) (2015) 1862–1870, https://doi.org/10.1021/AR500466U.

[48] X. Yang, Z. Sun, T. Low, H. Hu, X. Guo, F.J. García de Abajo, P. Avouris, Q. Dai, Nanomaterial-Based Plasmon-Enhanced Infrared Spectroscopy, Adv. Mater. 30 (20) (2018) 1704896.

[49] M. Majoube, M. Henry, Fourier Transform Raman and Infrared and Surface-Enhanced Raman Spectra for Rhodamine 6G, Spectrochim. Acta Part A Mol. Spectrosc. 47 (9–10) (1991) 1459–1466, https://doi.org/10.1016/0584-8539(91)80237-D.

[50] S. Shim, C.M. Stuart, R.A. Mathies, Resonance Raman Cross-Sections and Vibronic Analysis of Rhodamine 6G from Broadband Stimulated Raman Spectroscopy, ChemPhysChem 9 (5) (2008) 697–699.

[51] P. Hildebrandt, M. Stockburger, Surface-Enhanced Resonance Raman Spectroscopy of Rhodamine 6G Adsorbed on Colloidal Silver, J. Phys. Chem. 88 (24) (1984) 5935–5944, https://doi.org/10.1021/J150668A038.

[52] X.N. He, Y. Gao, M. Mahjouri-Samani, P.N. Black, J. Allen, M. Mitchell, W. Xiong, Y.S. Zhou, L. Jiang, Y.F. Lu, Surface-Enhanced Raman Spectroscopy Using Gold-Coated Horizontally Aligned Carbon Nanotubes, Nanotechnology 23 (20) (2012) 205702, https://doi.org/10.1088/0957-4484/23/20/205702.

[53] H. Xu, L. Xie, H. Zhang, J. Zhang, Effect of Graphene Fermi Level on the Raman Scattering Intensity of Molecules on Graphene, ACS Nano 5 (7) (2011) 5338–5344, https://doi.org/10.1021/nn103237x.

[54] N. Lisi, T. Dikonimos, F. Buonocore, M. Pittori, R. Mazzaro, R. Rizzoli, S. Marras, A. Capasso, Contamination-Free Graphene by Chemical Vapor Deposition in Quartz Furnaces, Sci. Rep. 7 (1) (2017) 9927, https://doi.org/10.1038/s41598-017-09811-z.

[55] W. Regan, N. Alem, B. Alemán, B. Geng, Ç. Girit, L. Maserati, F. Wang, M. Crommie, A. Zettl, A Direct Transfer of Layer-Area Graphene, Appl. Phys. Lett. 96 (11) (2010) 2–5, https://doi.org/10.1063/1.3337091.

[56] A. Capasso, M. De Francesco, E. Leoni, T. Dikonimos, F. Buonocore, L. Lancellotti, E. Bobeico, M.S. Sarto, A. Tamburrano, G. De Bellis, N. Lisi, Cyclododecane as Support Material for Clean and Facile Transfer of Large-Area Few-Layer Graphene, Appl. Phys. Lett. 105 (11) (2014) 113101, https://doi.org/

10.1063/1.4895733.
[57] A. Siokou, F. Ravani, S. Karakalos, O. Frank, M. Kalbac, C. Galiotis, Surface Refinement and Electronic Properties of Graphene Layers Grown on Copper Substrate: An XPS, UPS and EELS Study, Appl. Surf. Sci. 257 (23) (2011) 9785–9790, https://doi.org/10.1016/j.apsusc.2011.06.017.
[58] M.G. Helander, M.T. Greiner, Z.B. Wang, Z.H. Lu, Pitfalls in Measuring Work Function Using Photoelectron Spectroscopy, Appl. Surf. Sci. 256 (8) (2010) 2602–2605, https://doi.org/10.1016/J.APSUSC.2009.11.002.
[59] J.P. Perdew, K. Burke, M. Ernzerhof, Generalized Gradient Approximation Made Simple, Phys. Rev. Lett. 77 (18) (1996) 3865–3868, https://doi.org/10.1103/PhysRevLett.77.3865.
[60] J.P. Perdew, M. Ernzerhof, K. Burke, Rationale for Mixing Exact Exchange with Density Functional Approximations, J. Chem. Phys. 105 (22) (1996) 9982–9985, https://doi.org/10.1063/1.472933.
[61] B. Delley, An All-Electron Numerical Method for Solving the Local Density Functional for Polyatomic Molecules, J. Chem. Phys. 92 (1) (1990) 508–517, https://doi.org/10.1063/1.458452.
[62] B. Delley, From Molecules to Solids with the DMol3 Approach, J. Chem. Phys. 113 (18) (2000) 7756–7764, https://doi.org/10.1063/1.1316015.
[63] BIOVIA. Dassault Systèmes, Material Studio 2020. San Diego: Dassault Systèmes 2019.